DYNAMIC AND QUASI-STATIC CRUSH TESTING OF CLOSED CARBON-FIBRE/EPOXY ELEMENTS

A. Jackson*, M. David, A.J. Gunnion***, D. Kelly* and S. Dutton***
*School of Mechanical & Manufacturing Engineering, University of New South Wales
**Deutsches Zentrum für Luft-und Raumfahrt (DLR), Institute of Structures and Design
***Cooperative Research Centre for Advanced Composite Structures (CRC-ACS)

Keywords: *crashworthy design, energy absorption, composites, crush, joints*

Abstract

Crashworthiness of composite structures is of significant interest to manufacturers and operators as composites become more commonly used in automobiles and aircraft. Experimental crush testing remains an important tool in the design of subfloor fuselage structures for crashworthiness, as numerical simulations are still largely unable to accurately predict the crushing response of complex composite structures. In this paper, dynamic and quasi-static crush testing of carbon-fibre/epoxy specimens representative of elements in an energy-absorbing subfloor structure is reported. The elements were assembled using different joining methods, and the crush performance and fracture behaviour of the various designs are compared. Co-curing or co-bonding the element in one piece was shown to be the best design for maximising energy absorption, however the performance difference between all designs was narrower under dynamic conditions.

1 Introduction

Since the 1970's there has been considerable interest in the crashworthiness of composite materials, driven mainly by the increasing use of these materials in automobiles and aircraft. It is desirable from a crashworthiness perspective for designated areas of structures to fail in a progressive manner, thereby reducing the maximum acceleration on occupants so as to eliminate injuries and fatalities in relatively mild impacts, and minimise them in all severe but survivable accidents [1].

Failure by progressive crushing differs from catastrophic failure modes in that a stable region of failure exists over which the crushing load is approximately constant. Progressive failure of composites is usually achieved by applying a compressive load to a suitably-triggered component. Triggering generally involves a geometric gradient feature in the component which causes locally high stress relative to the rest of the part. The high local stress initiates microfracture in the triggered region [2], which progresses through the gradient feature, and eventually forms a stable crush zone.

Much work has been performed on the static and dynamic axial crushing of open and closed sections made from composite materials, such as in [3-15]. These studies have focused on the effect of matrix and fibre properties, geometry, loading rates and triggering mechanisms. Farley [16] described three main progressive failure modes, these being transverse shearing, lamina bending and local buckling. The first two of these failure modes have become more commonly referred to as fragmentation and splaying modes respectively [2, 7, 12, 17] and are typically observed in brittle fibre-reinforced materials.

While full scale testing of fuselage or sub-floor sections is often undertaken, such as in [18-21], it is expensive and time consuming. Alternatively, elements of a structure such as sections of beams or intersections of components can be tested. The importance of joints between sections in subfloor structures (i.e. structural 'hardpoints') in the overall crash response of aircraft or rotorcraft fuselages is well known to researchers who have

investigated sub-elements such as cruciform joints [21-23]. This current work sought to characterise the specific role of different assembly methods by isolating the joint in a relatively simple structure.

Previous testing [24] has investigated the quasi-static crush response of specimens designed by the Deutsches Zentrum für Luft- und Raumfahrt (DLR; German Aerospace Centre). This work extends previous studies by incorporating assembly details, such as bondlines and fastener rows, into the crush specimen. These specimens, made by joining modified DLR crush segments back-to-back or to a flat plate, have been tested quasi-statically and dynamically. Of specific interest is the effect of assembly method on energy absorption, as well as the relative dynamic versus quasi-static crush performance. The combined response of these elements in comparison to the single DLR crush segments is also examined.

2 Experimental Method

2.1 Manufacture of Elements

Crush specimens were manufactured from MTM44-1FR four-harness (4HS) and unidirectional (UNI) weave, 180°C cure, carbon-fibre pre-preg manufactured by Advanced Composites Group (ACG). Two different geometries of closed section elements were produced; back to back DLR sections (DLR-DLR) and DLR to Flat Plate sections (DLR-FP), shown in Figs. 1 and 2 respectively. A chamfer was machined into the top edge of all specimens to promote stable progressive crushing. Four different manufacturing methods were used to form the closed sections:

1. Co-curing the entire specimen in one cycle (referred to as Co-Cured (CC)).
2. Co-curing the entire specimen in one cycle with the addition of a 150 gsm FM300M film adhesive at the mid-plane (referred to as Co-Cured with Adhesive (CCA)).
3. Curing the two halves of the specimen separately, then bonding and fastening the two halves together using Hysol 9309 NA epoxy adhesive and CherryLock 1/8” rivets (referred to as Fasten-Bonded (FB)).
4. Curing the two halves of the specimen separately, with a proprietary thermoplastic film co-cured onto the surfaces to be joined, then welding the two halves together through these surfaces using heat and pressure. The joining process is known as Thermoset Composite Welding (TCW) [25] and is the subject of a number of patents and patent applications held by CRC-ACS.

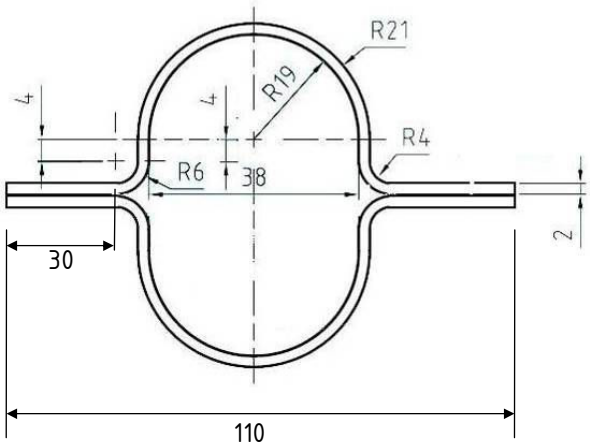

Fig. 1. DLR – DLR specimen cross-section

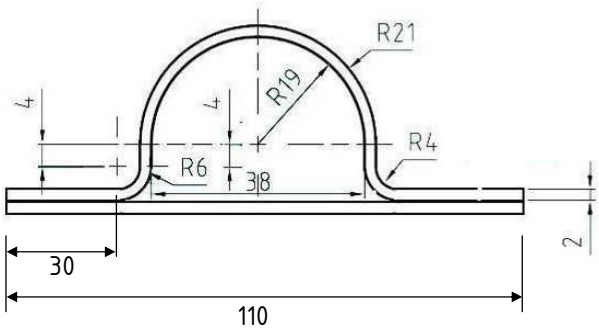

Fig. 2. DLR – FP specimen cross-section

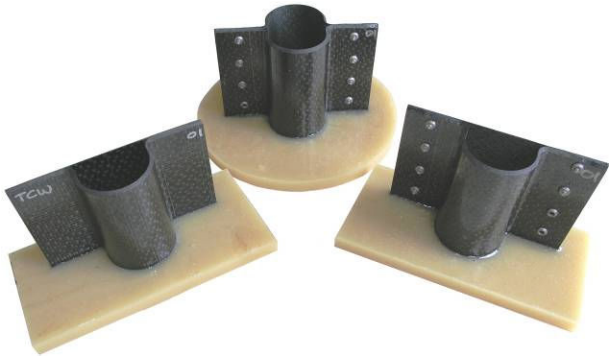

Fig. 3. Manufactured specimens

2.2 Test Method

Quasi-static testing was performed in an Instron universal test machine at 5 mm/min for the first 20 mm of crush displacement, then 20 mm/min to the final crush distance of 50 mm.

Dynamic testing was performed in an Instron VHS 20/100 high strain rate test machine, with an impact velocity of 8.5 m/s and a total crush distance of 50 mm.

3 Results and Discussion

A list of all the specimens produced and tested both quasi-statically (QS) and dynamically (DY) is provided in Table 1. Stable, progressive crushing was initiated and sustained in all specimens. The typical quasi-static and dynamic load – displacement response observed is shown in Fig. 4. Dynamic testing regimes produced a lower and more stochastic load response than quasi-static tests of equivalent specimens.

Table 1. Test Matrix

Joint Type	Specimen Geometry	Material [Lay-up]	No. Tested	
			QS	DY
FB	DLR-DLR	4HS $[0/90]_{2S}$	2	2
FB	DLR-FP	4HS $[0/90]_{2S}$	2	2
FB	DLR-DLR	4HS $[+45/-45]_{2S}$	2	-
FB	DLR-FP	4HS $[+45/-45]_{2S}$	2	-
FB	DLR-DLR	UNI $[0/90]_{3S}$	2	-
FB	DLR-FP	UNI $[0/90]_{3S}$	2	-
CC	DLR-DLR	4HS $[0/90]_{2S}$	2	1
CC	DLR-FP	4HS $[0/90]_{2S}$	2	1
CCA	DLR-DLR	4HS $[0/90]_{2S}$	2	1
CCA	DLR-FP	4HS $[0/90]_{2S}$	2	1
TCW	DLR-DLR	4HS $[0/90]_{2S}$	1	1
TCW	DLR-FP	4HS $[0/90]_{2S}$	1	1

Total energy absorption was calculated by integrating the test data for the entire test period (0 to ~50 mm displacement). This was then divided by the weight of the crushed portion of the specimen to give the Specific Energy Absorption (SEA) for each test. The weight of the crushed portion of specimen was calculated by multiplying the total crush distance by the mass per length of each specimen which was determined from pre-test measurements. Steady State Crush Force (SSCF) was calculated as the mean load for the test period from 3 mm vertical displacement to the end of the test. Steady State Crush Stress (SSCS) for a given test was calculated as the SSCF divided by the measured pre-test cross-sectional area, and is a useful means of comparing specimens with different numbers of plies.

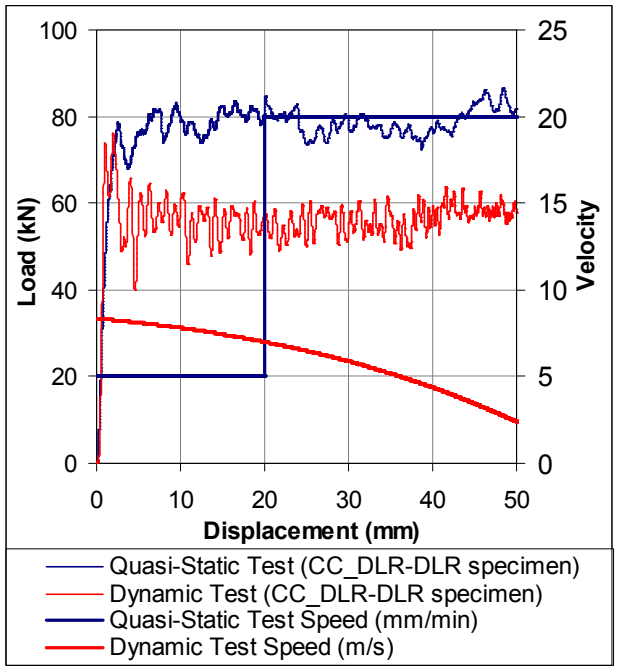

Fig. 4. Typical load – displacement curves

3.1 Quasi-Static Testing

Steady state crushing was obtained for all specimens tested quasi-statically. Specimens failed in the splaying failure mode where axial splitting occurs, forming fronds of crushed material which splay outwards and inwards at the crushing surface. A debris wedge forms at the laminate mid-plane which is driven down as the crush front progresses, causing an axial crack which progresses a certain distance ahead of the crushing surface. Pictures of typical 4HS $[0/90]_{2S}$ DLR-DLR and DLR-FP specimens (respectively) after crushing are provided in Figs. 7 and 8. Note that, around the curved section of the specimens, fronds have formed through splitting of the laminate at the mid-plane. However where the two flanges meet, the splitting changes such that the two specimen halves have split to form the fronds. For the DLR-FP specimens, the 'flat plate' section of

the specimen crushed progressively outwards as one large piece.

The failure mode of the 4HS $[+45/-45]_{2S}$ specimens was different to that described above. The angled orthotropic lay-up prevented the axial splitting forming to the same degree, and although crushed material was bent over at the crushing surface, fronds did not form to the same extent (see Fig. 9). This also resulted in larger sections of the laminate being separated from the specimen through cracking along the 45° axis, thus not being completely crushed.

The failure mode of the UNI $[0/90]_{3S}$ specimens was also markedly different. The specimens still failed in splaying mode as the 4HS specimens did, with the unidirectional hoop (90°) plies fracturing and axial splitting occurring to form fronds mainly comprising fractured 0° plies. When the crushing platen was raised after each test these fronds sprang back up (see Fig. 10 and 11) much more than those in the 4HS specimens, suggesting that less fibre breakage had occurred.

A summary of the quasi-static test results can be found in Table 2. As expected the DLR-DLR sections typically showed higher crush loads (average 27%) and higher SEA (average 20%) than the DLR-FP sections for comparable lay-ups and joint types. The less than desirable failure mode of the 4HS $[+45/-45]_{2S}$ specimens was reflected in lower crushing load and SEA. Specific performance (i.e. SSCS and SEA) of the UNI $[0/90]_{3S}$ specimens was lower than the 4HS $[0/90]_{2S}$ specimens, suggesting that although both configurations had orthotropic lay-up and same fibres and resin, the unidirectional plies are less efficient at absorbing energy than the woven 4HS ones.

As can be seen in Table 2, the FB joined sections had the highest crush loads, followed by the CC and CCA sections (which showed very similar performance) and finally the TCW sections. However, in terms of specific performance (i.e. SSCS and SEA) the CC and CCA sections showed the best performance followed by the FB and TCW sections. The weight of the fasteners and slightly higher cured ply thickness of the FB specimens were the reasons for the drop in performance when considering the specific parameters.

3.2 Dynamic Testing

A summary of the dynamic test results are shown in Table 3. The dynamically-tested 4HS $[0/90]_{2S}$ specimens failed in a similar manner to those tested quasi-statically, i.e. more debris was ejected from the specimen during the test. However the final crushed specimen still exhibited the same evidence of the splaying failure mode (i.e. fronds and debris wedge, see Figs. 12 to 14). It is unclear whether the failure mode is the same for the duration of the dynamic test, due to the large amount of debris ejected obscuring the view of the high speed camera. So it is possible that the specimen is initially failing in the fragmentation mode before changing to the splaying mode as the velocity decreases towards the end of the test.

In a reversal of the quasi-static trend, the TCW specimens had the highest SEA when comparing the average of the DLR-DLR and DLR-FP configurations for each assembly type. That the TCW specimens had significantly smaller reductions in crushing loads and SEA between quasi-static and dynamic test conditions suggests that the TCW interface has relatively higher Mode I fracture properties at higher strain rates compared to the other joint interfaces. With the other specimens (FB, CC and CCA types) the reduction in SEA was in the range 25% – 29% for the DLR-DLR type, an interestingly higher knockdown than the range 21% – 23% observed for the DLR-FP group.

3.3 Analysis of Segment Contributions

The breakdown of the different segments of the DLR-DLR and DLR-FP specimens is shown in Fig. 5. Standard DLR crush segments comprise just the curved ‘omega’ shaped section of the closed elements. Quasi-static crush tests of these segments were performed, using the same material and lay-up of the closed sections.

It was therefore possible to analyse the contributions of the different segments of the combined specimens with respect to the single DLR geometry. Firstly the crush results of the standard DLR segments were subtracted from the DLR-DLR results to give the predicted contribution of the flange sections of these elements. Secondly, using this predicted flange

contribution and the single DLR results, the theoretical contribution of the flat-plate section of the DLR-FP specimens could be calculated.

A summary of these theoretical predictions (in terms of SSCF) is shown in Fig. 15. For the DLR-DLR specimens, the DLR segments are contributing between 58% and 80% of each specimen's total crushing load. For the DLR-FP the DLR segments contribute between 35% and 58% and the FP section between 3% and 30%. The analysis of the DLR-FP specimens assumes that the contribution of the flange is the same as that from the equivalent DLR-DLR specimen. Thus, this analysis does not take into account the fact that the interaction between the flanges and the central portion of the specimen is different between the DLR-DLR and DLR-FP geometries, and hence may be tenuous.

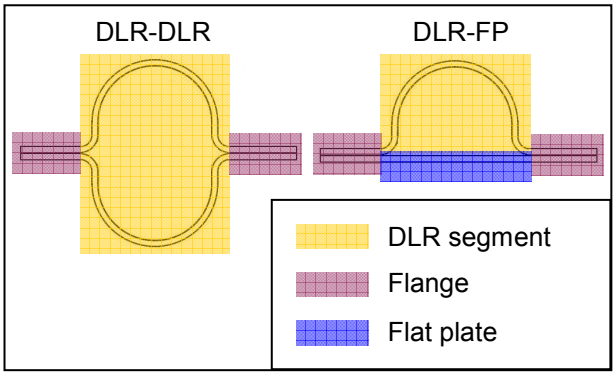

Fig. 5. Segments of specimens

3.4 Effect of Joint on Crush Performance

When considering all the DLR-DLR 4HS $[0/90]_{2S}$ specimens as a group to compare the joint crush performance, the FB specimens consistently sustained a higher crushing load than the other assembly types. However, with the weight of the fasteners included in the specimen mass, the SEA of these specimens was lower than the CC and CCA types. The CC and CCA assembly techniques are closely related, and unsurprisingly produced very similar results to each other under quasi-static and dynamic conditions.

Strain rate can influence the fracture toughness of carbon-epoxy, adhesives and thermoplastics, e.g. [26-29]. However, it is difficult to draw definitive trends from the literature because the results are sensitive to particular material properties and the strain rates used in the tests.

Fig. 6 shows the reduction in SEA for quasi-static to dynamic conditions. Quasi-static and dynamic testing of standard DLR specimens using the same material revealed a SEA decrease of 15%. This is compared to a quasi-static to dynamic reduction in SEA for the DLR-DLR specimens of between 20% to 29%, implying that the crushing of the flange material and Mode-I splitting of the assembly interface is relatively less efficient under dynamic conditions.

The TCW assembly technique performed relatively much better under dynamic conditions compared to the other joint types. Under dynamic testing the crush load was approximately equivalent to both the CC and CCA techniques, with the SEA being only 3% lower. This is compared to the quasi-static tests where it was down 14% and 16% respectively in both measures.

Although only a limited number of specimens have been tested, it can be concluded that the CC, CCA and TCW methods all offer very similar dynamic SEA performance; a critical design parameter for crashworthy aeronautical structures. Using the current data, a final decision between these three assembly techniques could be based more upon manufacturing and assembly costs.

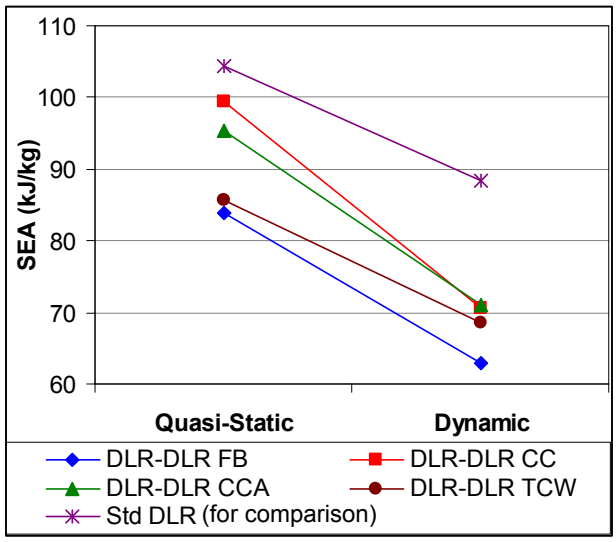

Fig. 6. Quasi-static to dynamic SEA reduction

Fig. 7. CC DLR-DLR 4HS $[0/90]_{2S}$ (QS)

Fig. 8. CC DLR-FP 4HS $[0/90]_{2S}$ (QS)

Fig. 9. FB 4HS $[\pm 45]_{2S}$ (QS), (L) DLR-DLR, (R) DLR-FP

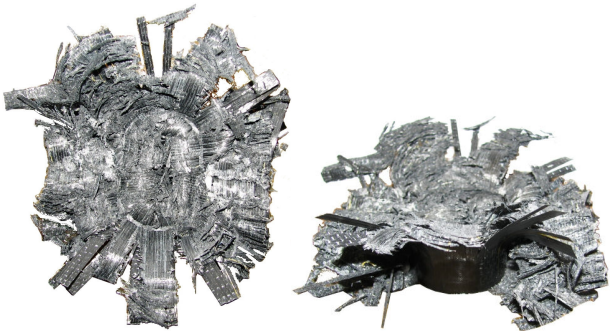

Fig. 10. FB DLR-DLR UNI $[0/90]_{3S}$ (QS)

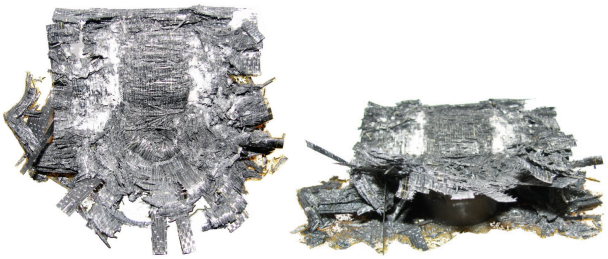

Fig. 11. FB DLR-FP UNI $[0/90]_{3S}$ (QS)

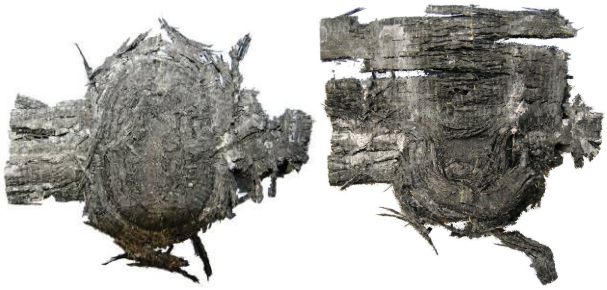

Fig. 12. FB 4HS $[0/90]_{2S}$ (DY), (L) DLR-DLR, (R) DLR-FP

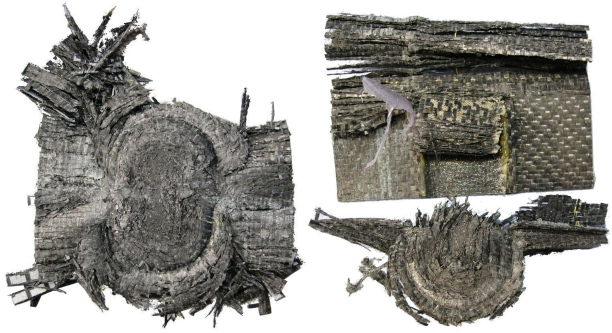

Fig. 13. CCA 4HS $[0/90]_{2S}$ (DY), (L) DLR-DLR, (R) DLR-FP

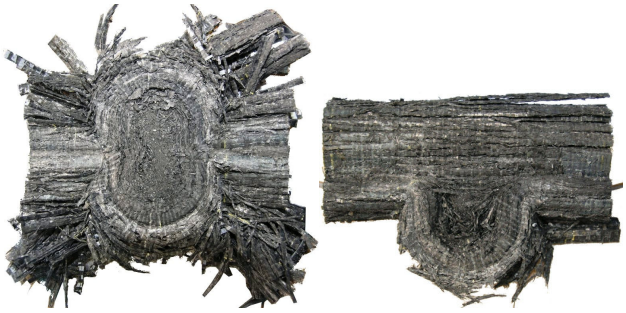

Fig. 14. TCW 4HS $[0/90]_{2S}$ (DY), (L) DLR-DLR, (R) DLR-FP

Table 2. Quasi-static test results

Joint Type	Geometry	Material [Lay-up]	Peak load (kN) [range]	SSCF (kN) [range]	SSCS (MPa) [range]	SEA (kJ/kg) [range]
FB	DLR-DLR	4HS $[0/90]_{2S}$	107.4 [6.9]	87.7 [1.2]	146 [2.1]	83.8 [0.4]
FB	DLR-FP	4HS $[0/90]_{2S}$	84.9 [3.2]	63.5 [4.9]	128 [10.4]	71.0 [1.4]
FB	DLR-DLR	4HS $[+45/-45]_{2S}$	83.2 [4.6]	52.4 [4.6]	88 [7.3]	45.4 [17.0]
FB	DLR-FP	4HS $[+45/-45]_{2S}$	71.2 [7.4]	50.1 [0.3]	102 [1.6]	55.8 [0.6]
FB	DLR-DLR	UNI $[0/90]_{3S}$	99.4 [4.0]	81.0 [0.5]	126 [0.9]	75.3 [0.3]
FB	DLR-FP	UNI $[0/90]_{3S}$	79.4 [14.8]	59.0 [3.1]	110 [4.1]	59.4 [6.1]
CC	DLR-DLR	4HS $[0/90]_{2S}$	88.5 [3.9]	80.2 [3.7]	157 [11.7]	99.4 [3.3]
CC	DLR-FP	4HS $[0/90]_{2S}$	75.2 [6.6]	60.1 [0.2]	134 [0.4]	75.7 [0.9]
CCA	DLR-DLR	4HS $[0/90]_{2S}$	84.4 [0.4]	77.8 [1.5]	156 [5.1]	95.3 [2.3]
CCA	DLR-FP	4HS $[0/90]_{2S}$	79.5 [4.8]	60.3 [5.3]	140 [11.1]	75.4 [2.0]
TCW	DLR-DLR	4HS $[0/90]_{2S}$	75.8 [N/A]	67.5 [N/A]	147 [N/A]	85.7 [N/A]
TCW	DLR-FP	4HS $[0/90]_{2S}$	58.8 [N/A]	47.1 [N/A]	110 [N/A]	69.7 [N/A]

Table 3. Dynamic test results

Joint Type	Geometry	Material [Lay-up]	Peak load (kN) [range]	SSCF (kN) [range] (reduction from QS)	SSCS (MPa) [range]	SEA (kJ/kg) [range] (reduction from QS)
FB	DLR-DLR	4HS $[0/90]_{2S}$	90.8 [3.4]	64.0 [1.1] (27.1%)	127 [2.3]	62.9 [1.1] (25.0%)
FB	DLR-FP	4HS $[0/90]_{2S}$	78.5 [10.6]	48.1 [1.6] (24.3%)	109 [3.7]	56.0 [0.9] (21.1%)
CC	DLR-DLR	4HS $[0/90]_{2S}$	76.2 [N/A]	56.4 [N/A] (29.6%)	109 [N/A]	70.6 [N/A] (28.9%)
CC	DLR-FP	4HS $[0/90]_{2S}$	75.0 [N/A]	42.7 [N/A] (28.9%)	95 [N/A]	58.5 [N/A] (22.8%)
CCA	DLR-DLR	4HS $[0/90]_{2S}$	88.5 [N/A]	57.6 [N/A] (25.9%)	115 [N/A]	71.0 [N/A] (25.5%)
CCA	DLR-FP	4HS $[0/90]_{2S}$	76.3 [N/A]	44.1 [N/A] (26.9%)	99 [N/A]	58.7 [N/A] (22.1%)
TCW	DLR-DLR	4HS $[0/90]_{2S}$	85.1 [N/A]	56.2 [N/A] (16.9%)	121 [N/A]	68.6 [N/A] (20.0%)
TCW	DLR-FP	4HS $[0/90]_{2S}$	63.1 [N/A]	43.0 [N/A] (8.7%)	107 [N/A]	62.6 [N/A] (10.1%)

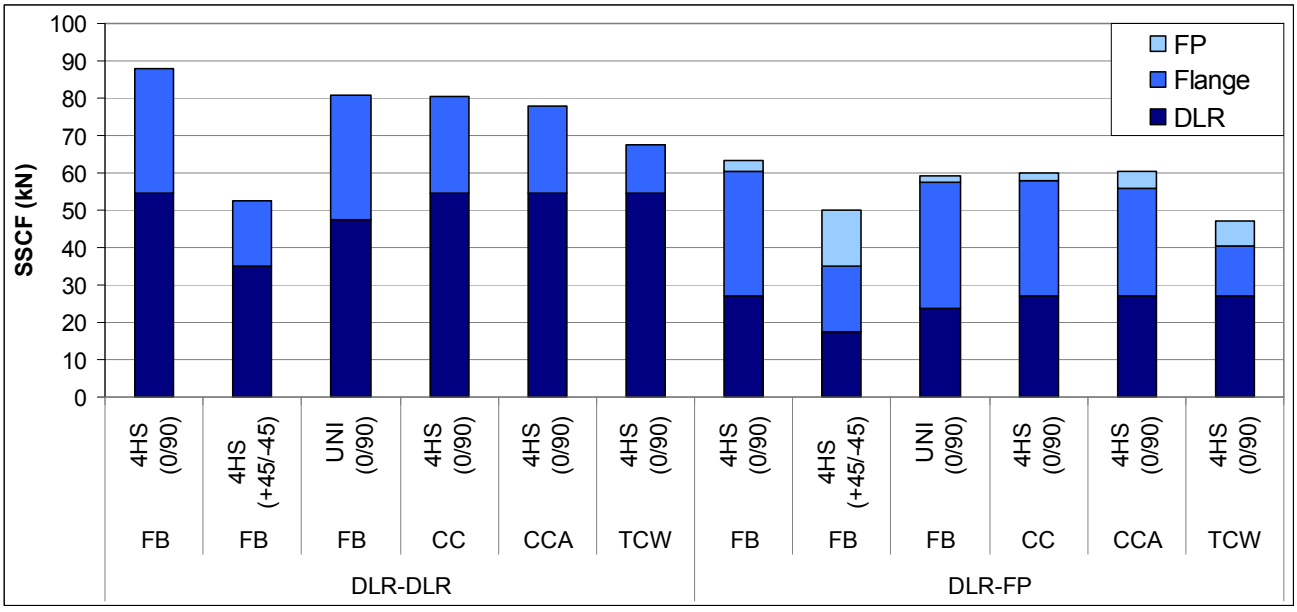

Fig. 15. Contributions of specimen features to overall crush load (quasi-static)

4 Conclusions

Dynamic and quasi-static crush testing has been undertaken of carbon-fibre/epoxy specimens representative of elements in a crashworthy, energy-absorbing subfloor structure. Two specimen geometries were tested, and all were assembled using different joining methods; fastening and bonding, co-curing, co-bonding and TCW.

The DLR-DLR geometry performed much better than DLR-FP geometry in all cases. For the design of similar features in an energy-absorbing structure, using symmetry and avoiding flat sections in planes perpendicular to the crushing direction would be recommended. The latter appear to crush less efficiently than curved sections.

A reduction in SEA of between 10% and 30% from quasi-static to dynamic loading was seen across all cases. The TCW joined specimens showed the smallest reduction in performance between the two loading cases.

If a high crush load is desirable, then fastening and bonding of components could provide the best solution. However, specific performance is a more relevant indicator for energy absorbing structures in aeronautical design, and the CC, CCA and TCW assembly techniques all showed very similar dynamic SEA, and the choice between the three methods could come down to other variables such as manufacturing and assembly costs.

Acknowledgements

This work is part of the research program of the Cooperative Research Centre for Advanced Composite Structures, and was conducted under the Helicopter Research Program project, Design for Crashworthiness. The authors wish to acknowledge the support and guidance of the project team from the CRC-ACS, University of New South Wales, Pacific ESI, Defence Science and Technology Organisation, Australian Aerospace and the Deutsches Zentrum für Luft- und Raumfahrt (DLR). In particular the support and testing facilities provided by Dr Alastair Johnson and his colleagues of the DLR Institute for Structures and Design is greatly appreciated. The first author also acknowledges financial support provided through the Australian Postgraduate Award and the CRC-ACS. The authors also wish to thank the Advanced Composites Group Limited (UK) for providing materials for use in the work presented in this paper.

References

[1] Zimmermann RE and Merritt NA. Aircraft crash survival design guide, Vol. 1. *USAAVSCOM TR 89-D-22A* 1989, Fort Eustis: Simula Inc.

[2] Ramakrishna S. Microstructural design of composite materials for crashworthy structural applications. *Materials & Design,* Vol. 18, No. 3, pp. 167-173, 1997.

[3] Farley GL and Jones RM. Energy absorption capability of composite tubes and beams. *NASA Technical Memorandum 101634* 1989, Hampton: U.S. Army Aviation Research and Technology Activity - AVSCOM.

[4] Hamada H, Ramakrishna S and Sato H. Effect of fiber orientation on the energy absorption capability of carbon fiber/PEEK composite tubes. *J Compos Mater,* Vol. 30, No. 8, pp. 947-63, 1996.

[5] Mamalis AG, Manolakos DE, Ioannidis MB and Papapostolou DP. On the response of thin-walled CFRP composite tubular components subjected to static and dynamic axial compressive loading: experimental. *Compos Struct,* Vol. 69, No. 4, pp. 407-420, 2005.

[6] Melo JDD, Silva ALS and Villena JEN. The effect of processing conditions on the energy absorption capability of composite tubes. *Compos Struct,* Vol. 82, No. 4, pp. 622-628, 2008.

[7] Ramakrishna S and Hull D. Energy absorption capability of epoxy composite tubes with knitted carbon fibre fabric reinforcement. *Compos Sci Technol,* Vol. 49, No. 4, pp. 349-356, 1993.

[8] Sigalas I, Kumosa M and Hull D. Trigger mechanisms in energy-absorbing glass cloth/epoxy tubes. *Compos Sci Technol,* Vol. 40, No. 3, pp. 265-287, 1991.

[9] Solaimurugan S and Velmurugan R. Influence of fibre orientation and stacking sequence on petalling of glass/polyester composite cylindrical shells under axial compression. *International Journal of Solids and Structures,* Vol. 44, No. 21, pp. 6999-7020, 2007.

[10] Song H-W, Du X-W and Zhao G-F. Energy absorption behavior of double-chamfer triggered glass/epoxy circular tubes. *J Compos Mater,* Vol. 36, No. 18, pp. 2183-2198, 2002.

[11] Tao WH, Robertson RE and Thornton PH. Effects of material properties and crush conditions on the crush

energy absorption of fiber composite rods. *Compos Sci Technol,* Vol. 47, No. 4, pp. 405-418, 1993.
[12]Hull D. A unified approach to progressive crushing of fibre-reinforced composite tubes. *Compos Sci Technol,* Vol. 40, No. 4, pp. 377-421, 1991.
[13]Thornton PH. Energy absorption in composite structures. *J Compos Mater,* Vol. 13, No. 3, pp. 247-262, 1979.
[14]Thuis HGSJ and Metz VH. Influence of trigger configurations and laminate lay-up on the failure mode of composite crush cylinders. *Compos Struct,* Vol. 25, No. 1-4, pp. 37-43, 1993.
[15]Bisagni C. Experimental investigation of the collapse modes and energy absorption characteristics of composite tubes. *Int J Crashworthiness,* Vol. 14, No. 4, pp. 365 - 378, 2009.
[16]Farley GL and Jones RM. Crushing characteristics of continuous fiber-reinforced composite tubes. *J Compos Mater,* Vol. 26, No. 1, pp. 36-50, 1992.
[17]Ramakrishna S and Hamada H. Energy absorption characteristics of crash worthy structural composite materials. *Key Eng Mater,* Vol. 141-143, No. Pt 2, pp. 585-620, 1998.
[18]Fasanella EL, Jackson KE, Lyle KH, Sparks CE and Sareen AK. Multi-terrain impact tests and simulations of an energy absorbing fuselage section. *J American Helicopter Soc,* Vol. 52, No. 2, pp. 159-168, 2007.
[19]Jackson KE. Impact Testing and Simlation of a Crashworthy Composite Fuselage. In: *American Helicopter Society 56th Annual Forum*. Virginia Beach, Virginia: US Army Research Laboratory, 2000.
[20]Jackson KE, Fuchs YT and Kellas S. Overview of the National Aeronautics and Space Administration Subsonic Rotary Wing Aeronautics Research Program in Rotorcraft Crashworthiness. *Journal of Aerospace Engineering,* Vol. 22, No. 3, pp. 229-239, 2009.
[21]Johnson AF, Kindervater CM and Jackson KE. Multifunctional design concepts for energy absorbing composite fuselage sub-structures. *Annual Forum Proceedings - American Helicopter Society*, Vol. 2. Virginia Beach, VA, USA: American Helicopter Soc, Alexandria, VA, USA, 1997. p. 1115-1128
[22]Bisagni C and Mirandola C. Experimental and numerical investigation of crash behavior of composite helicopter cruciform elements. *J American Helicopter Soc,* Vol. 50, No. 1, pp. 107-116, 2005.
[23]Kindervater CM, Kohlgruber D and Johnson A. Composite vehicle structural crashworthiness - A status of design methodology and numerical simulation techniques. *Int J Crashworthiness,* Vol. 4, No. 2, pp. 213 - 230, 1999.
[24]Jackson A, Dutton S, Gunnion AJ and Kelly D. Effect of manufacture and laminate design on energy absorption of open carbon-fibre/epoxy sections. *ICCM-17 (CD-ROM)*. Edinburgh, UK: IOM Communications Ltd, 2009.
[25]Paton R, Hou M, Beehag A and Falzon P. A breakthrough in the assembly of aircraft composite structures. *25th Congress of the Internaltional Council of the Aeronautical Sciences (ICAS)*. Hamburg, Germany: ICAS, 2006.
[26]Fracasso R, Rink M, Pavan A and Frassine R. The effects of strain-rate and temperature on the interlaminar fracture toughness of interleaved PEEK/CF composites. *Compos Sci Technol,* Vol. 61, No. 1, pp. 57-63, 2001.
[27]Jacob GC, Starbuck JM, Fellers JF, Simunovic S and Boeman RG. The effect of loading rate on the fracture toughness of fiber reinforced polymer composites. *J App Polym Sci,* Vol. 96, No. 3, pp. 899-904, 2005.
[28]Carlberger T, Biel A and Stigh U. Influence of temperature and strain rate on cohesive properties of a structural epoxy adhesive. *International Journal of Fracture,* Vol. 155, No. 2, pp. 155-166, 2009.
[29]Chiu WK, Chalkley PD and Jones R. Effects of temperature on the shear stress-strain behaviour of structural adhesives (FM73). *Computers & Structures,* Vol. 53, No. 3, pp. 483--489, 1994.

Contact Author Email Address

Adrian Jackson: a.jackson@crc-acs.com.au

Copyright Statement